Available online at www.sciencedirect.com
ScienceDirect
Journal of Power Sources 169 (2007) 167–176
JOURNAL OF POWER SOURCES
www.elsevier.com/locate/jpowsour

# Zirconia supported catalysts for bioethanol steam reforming: Effect of active phase and zirconia structure☆

M. Benito*, R. Padilla, L. Rodríguez, J.L. Sanz, L. Daza

*Instituto de Catálisis y Petroleoquímica (CSIC), C/ Marie Curie 2, Campus Cantoblanco, 28049 Madrid, Spain*

Available online 3 February 2007

**Abstract**

Three new catalysts have been prepared in order to study the active phase influence in ethanol steam reforming reaction. Nickel, cobalt and copper were the active phases selected and were supported on zirconia with monoclinic and tetragonal structure, respectively. To characterize the behaviour of the catalysts in reaction conditions a study of catalytic activity with temperature was performed. The highest activity values were obtained at 973 K where nickel and cobalt based catalysts achieved an ethanol conversion of 100% and a selectivity to hydrogen close to 70%. Nickel supported on tetragonal zirconia exhibited the highest hydrogen production efficiency, higher than 4.5 mol $H_2$/mol EtOH fed. The influence of steam/carbon (S/C) ratio on product distribution was another parameter studied between the range 3.2–6.5. Nickel supported on tetragonal zirconia at S/C = 3.2 operated at 973 K without by-product production such as ethylene or acetaldehyde. In order to consider a further application in an ethanol processor, a long-term reaction experiment was performed at 973 K, S/C = 3.2 and atmospheric pressure. After 60 h, nickel supported on tetragonal zirconia exhibited high stability and selectivity to hydrogen production.


*Keywords:* Bioethanol; Reforming; Bio-energy; Hydrogen; Fuel processor; Fuel cell

## 1. Introduction

Hydrogen is a clean and free carbon energy vector that can be used directly in thermal combustion engines or converted into electrical energy by fuel cells. The advantages of fuel cells in comparison with other energy systems, come from the fact that their efficiency is much higher than other energy systems. This is so, as they are not submitted to a Carnot cycle and water is only obtained as final product [1]. The development of fuel cells as a very profitable technology is inevitably linked to the development of efficient fuel processing systems to obtain hydrogen, the most valuable fuel for this type of devices. These advantages may represent the key to diminish the environmental problems by reducing the greenhouse effect and therefore the earth global warming effect.

To achieve these environmental goals, it is indispensable to produce hydrogen in a clean way. Nowadays, hydrogen is obtained from hydrocarbon reforming (85% natural gas steam reforming) and electrolysis processes, the last one with very low efficiency [2]. As fossil fuels have carbon atoms in its composition, its steam reforming produces carbon oxides that contribute to greenhouse effect, therefore fuel reforming is not a great advance to solve environmental problems [3].

An attractive option to obtain hydrogen is to use renewable energy sources. In this way, ethanol obtained from biomass fermentation (farm remainders, crops, etc.), is an optimum candidate to be used as a hydrogen source [4]. Due to its origin, bioethanol is a renewable energy source because it is obtained from plants that can capture carbon dioxide produced in bioethanol reforming process. The advantages of bioethanol in contrast to other alcohols such as methanol, come from the fact that ethanol is easier to store because of its lower volatility. The toxicity is an important aspect to be considered, on account of the fuel will be handled to be transported and in refuelling operations. From this standpoint, ethanol presents much lower toxicity than other alcohols and fuels. Taking into consideration economical and logistic aspects, ethanol could be delivered in a distribution net similar to gasoline without any big changes [5]. The special characteristics of ethanol as an energy carrier could make the decentralized energy production easier, and could develop the local economy. An important problem to solve is to develop a specific ethanol reforming catalyst with

☆ This paper presented at the 2nd National Congress on Fuel Cells CONAPPICE 2006.

* Corresponding author. Tel.: +34 91 5854793; fax: +34 91 5854760.
*E-mail address:* mjbenito@icp.csic.es (M. Benito).

0378-7753/$ – see front matter © 2007 Elsevier B.V. All rights reserved.
doi:10.1016/j.jpowsour.2007.01.047

good skills in catalytic activity, selectivity, resistant to long-term operations.

Most of the catalysts reported in bibliography are based in nickel and cobalt as active phase, most commonly used in methane steam reforming, reforming technology with higher development and implantation level, and copper for methanol reforming. Nickel is very efficient to activate C–C bonds, important aspect in heavier alcohol reforming [6,7]. Nickel on acid support such as alumina, usually presents initial high activities but diminishes progressively due to deactivation problems. To avoid this fact, some authors have used other supports such as MgO or have introduced alkaline precursors on alumina to neutralize the acid sites [8,9]. This improves the stability but do not overcome the deactivation problems. Other authors have tried to mitigate the catalyst deactivation by carbon deposition by using cobalt as active phase [10,11]. The use of noble metal such as Pt, Rh or Pd has been tested [7,12,13], but the possibility of applying this type of catalyst is really difficult on account of the high price for noble metal based catalysts.

The aim of this work is to study the influence of nickel, cobalt and copper active phases supported on zirconia as well as the influence of zirconia structure, on catalytic activity for bioethanol steam reforming. Another goal is to try to overcome the problems associated to catalyst deactivation derived from surface acidity by using zirconia as support. In order to study its further implentation in a bioethanol processor, the response to long-term operation reaction experiments has been performed.

## 2. Experimental

### 2.1. Catalysis preparation

Two zirconia supports: $ZrO_2$ and $ZrO_2$ stabilized with $SiO_2$ were prepared from hydroxide precursors by calcination at 1073 K. The supports were heated at 5 K $min^{-1}$ to achieve the calcination set point and maintained 2 h at this temperature.

To study the influence of the active phase on catalytic activity, three active phases were selected: Ni, Co, Cu. These active phases were impregnated by incipient wetness impregnation method with a nitrate aqueous metal solution on zirconia supports. Nitrate precursor salts were $Ni(NO_3)_2{\cdot}6H_2O$, $Co(NO_3)_2{\cdot}6H_2O$, $Cu(NO_3)_2{\cdot}3H_2O$, respectively, supplied by Panreac. The impregnated catalyst samples were dried over night at 383 K and calcined at 1023 K in order to stabilize the active phase by removing the precursor salts.

Therefore, two series of catalysts were prepared with an active phase nominal composition of 10 wt% on the two zirconia supports, that were denoted as NiZr, CoZr, CuZr (Series 1) and NiZrSi, CoZrSi, CuZrSi (Series 2), respectively.

### 2.2. Characterization

The chemical composition of the catalysts, was analysed by inductively coupled plasma atomic emission spectroscopy (ICP-AES), using an Optima 3300DV Perkin-Elmer equipment.

Catalysts were characterized by XRD and the diffractograms were recorded following a step-scanning procedure (step-size 0.02°, 2$\theta$ scanning from 4° to 100° by a Seifert 3000P diffractometer coupled to an acquisition data system). The samples were analysed between 4° and 100° by using the radiation Cu K$\alpha$ ($\lambda = 0.15481$ nm). The identification of the crystallographic phases was performed by using the software PDFWIN. This software is based on diffraction data from International Centre for Diffraction Data. To calculate the particle size from XRD patterns, the Scherrer equation was applied.

Nitrogen adsorption–desorption isotherms were obtained at 77 K using an automatic system Micromeritcs ASAP 2100. The catalysts samples were previously out gassed at 423 K for 12 h. BET surface areas were calculated from isotherms by adjusting to Brunauer–Emmet–Teller mathematical expression.

Thermogravimetric experiments were performed with a Mettler-Toledo TGA/SDTA 851$^e$ thermobalance and experimental data were recorded with the software STAR 8.10. The catalyst samples were submitted to a reductive mixture $H_2/N_2$ (40% $H_2$) with a total flow 50 $cm^3$ $min^{-1}$. A nitrogen protective gas flow (50 $cm^3$ $min^{-1}$) was introduced in the thermobalance to perform the reduction experiments. The catalyst samples were heated to 1073 K at 10 K $min^{-1}$.

### 2.3. Reaction experiments

The reaction apparatus is equipped with mass flow controllers to adjust the pre-treatment gas flow and an isocratic pump to control the liquid feed with a very good accuracy. A SCADA software for data acquisition and control for the different reaction parameters was designed. A catalyst sample (100 mg) was introduced in a quartz reactor with a 9.52 mm of external diameter.

Chromatography was the analytical technique used to evaluate the composition of reaction products. To separate permanent gases ($H_2$, CO, $CO_2$ and $CH_4$), a 5 Å molecular sieve was used, while hydrocarbons were separated in a Porapak Q column. The chromatograph (Agilent 6890 N) is equipped with TCD and FID detectors connected in line. In order to identify possible steam reforming by-products, a mass spectrometer (Agilent 5973) connected to a GC chromatograph was used.

The ratio steam/carbon was studied in the range 3.2–6.5, the gas hourly space velocity (GHSV) was fixed at 76,000 $h^{-1}$ and the reaction temperature at 973 K. The experimental tests have been performed introducing bioethanol and water without a gas carrier in order to work in similar conditions expected in a real fuel processor.

The parameters used to study the catalytic activity were ethanol conversion, denoted as $X_{EtOH}$, and product distribution denoted as $Y_i$. These parameters were calculated by the following Eqs. (1) and (2):

$$X_{EtOH} = \frac{\text{mol EtOH}_{in} - \text{mol EtOH}_{out}}{\text{mol EtOH}_{in}} \times 100 \quad (1)$$

$$Y_i = \frac{\text{mol } P_i}{\sum_{i=1}^{n} \text{mol Pi}} \times 100 \quad (2)$$

$P_i$ is the reaction products.

Gas hourly space velocity (GHSV) was calculated by the following mathematical equation (3):

$$\mathrm{GHSV} = \frac{Q_{\mathrm{reactants}}}{V_{\mathrm{Catalytic\ bed}}} \quad (3)$$

## 3. Results

### 3.1. Characterization

Fig. 1a shows the nitrogen isotherm curve obtained for a zirconia sample at 77 K. The BET surface area calculated was 25 $m^2\ g^{-1}$. Zirconia sample exhibits an isotherm curve type IV H2 following the IUPAC criteria, characterized by mesopores. The hysteresis loop is associated to pore condensation. The porous distribution obtained presents two peaks at 34 and 22 nm for adsorption–desorption, respectively, dimensions that correspond to the body and the inlet pore diameter, respectively (Fig. 1b). The pores volume obtained is 0.1960 $cm^3\ g^{-1}$. Fig. 2a represents the nitrogen isotherm curve obtained for a zirconia stabilized with silica at 77 K. The BET surface area was 77 $m^2\ g^{-1}$. Zirconia stabilized sample presents an isotherm curve type IV H1. In this case, the pore diameter calculated is 4 nm, much lower value compared to zirconia sample (Fig. 1b), and the pores volume 0.1235 $cm^3\ g^{-1}$.

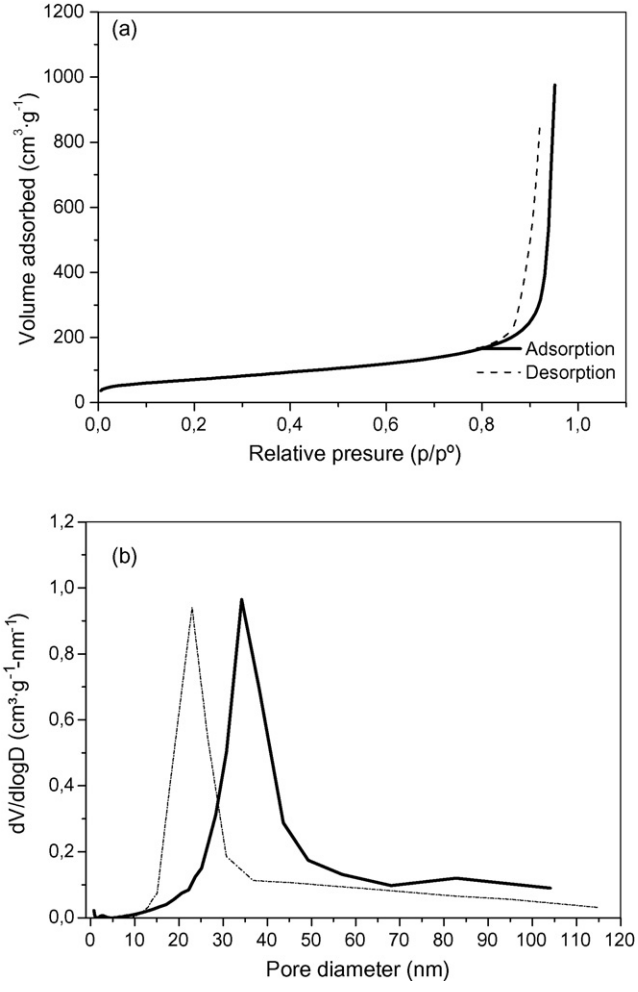


Fig. 1. $ZrO_2$ support: (a) nitrogen adsorption isotherm; (b) pore distribution.

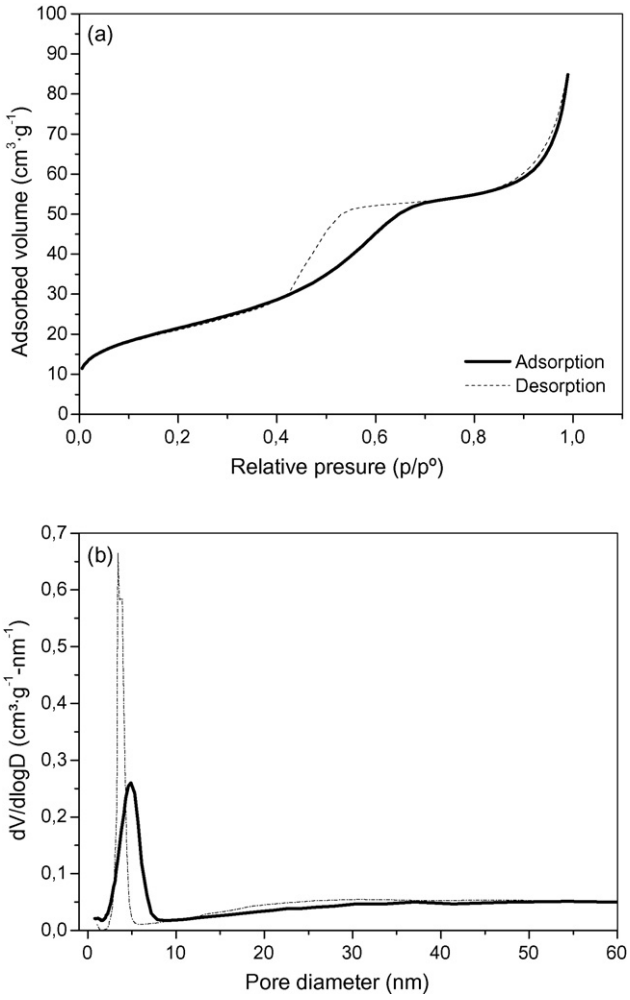


Fig. 2. $ZrO_2$–$SiO_2$ support: (a) nitrogen adsorption isotherm; (b) pore distribution.

Figs. 3 and 4 show the XRD diffractograms that correspond to $ZrO_2$ supported catalysts (Series 1) and $ZrO_2$ stabilized with

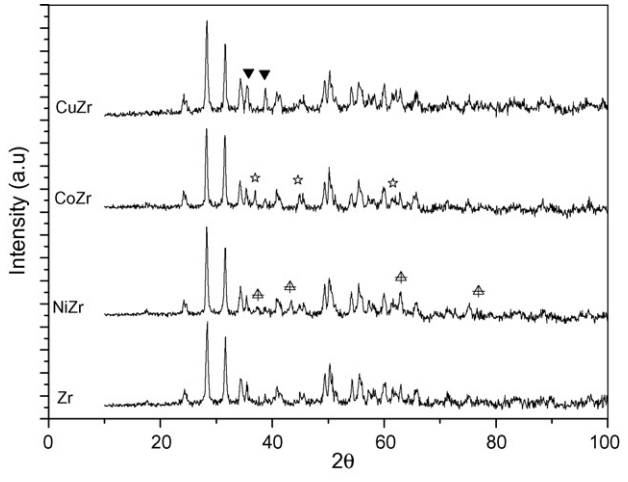


Fig. 3. XRD diffraction pattern obtained on zirconia supported samples: (☆) cubic $Co_2O_3$; (⏃) cubic NiO; (▼) CuO monoclinic.

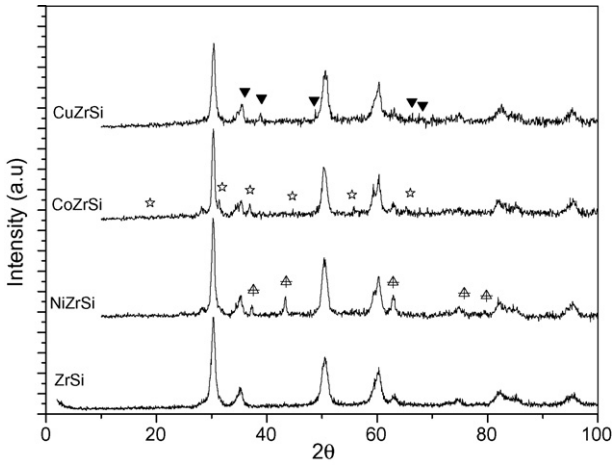


Fig. 4. XRD diffraction pattern obtained on zirconia stabilized with silica supported samples: (☆) cubic $Co_2O_3$; (⏃) cubic NiO; (▼) CuO monoclinic.

$SiO_2$ supported catalysts (Series 2), respectively. The diffraction peaks obtained for $ZrO_2$ were assigned to a monoclinic structure while the introduction of silica as stabilizer agent allowed obtaining a tetragonal structure.

The high concentration of active phase used to prepare the catalyst samples (10%) allows detecting the diffraction peaks that correspond to nickel, cobalt and copper oxides, where dispersions on zirconia (Series 1, Fig. 3) are not very high. On zirconia stabilized with silica (Fig. 4), the diffraction pattern shows higher particle size of nickel on the catalytic support, detected on account of the increase of the intensity of the peak assigned to nickel oxide. This presents a particle size of 30 nm (Table 1), very high value in comparison to copper particles (8 nm). Nickel and cobalt catalysts (Series 2) present a particle size higher than zirconia supported ones. Cobalt and copper oxides have been identified on zirconia stabilized support but the particle sizes for these samples are lower than for the nickel one, demonstrating that these samples present a higher dispersion.

Table 2 summarizes the temperatures that correspond to mass loss associated to active phase reduction are presented for every catalyst sample studied in thermogravimetric experiments. On NiZr, two reduction steps have been identified. The lower temperature corresponds to NiO free particles reduction and the higher temperature correspond to particles that present more interaction with the support [14]. For NiZrSi only one peak is detected at an intermediate temperature, that can be assigned to a higher interaction degree of the NiO particles with the support. XRD experiments confirm the presence of NiO particles of higher size (Table 1). For CoZr two peaks are detected (Table 2), the low temperature peak can be ascribed to surface

Table 1
Particle size calculated from XRD diffractograms

| | Particle size (nm) | |
|---|---|---|
| | Series 1 | Series 2 |
| Nickel | 20 | 31 |
| Cobalt | 15 | 18 |
| Copper | 17 | 8 |

Table 2
Temperature reduction obtained for catalyst samples in TG experiments

| | Reduction temperature (°C) | |
|---|---|---|
| | Series 1 | Series 2 |
| Nickel | 643<br>823 | 703 |
| Cobalt | 583<br>623 | 658 |
| Copper | 443<br>498 | 508 |

$Co_3O_4$ reduction while the high temperature peak corresponds to bulk reduction [15]. On CoZrSi only appears one reduction peak at higher temperature on account of a higher interaction with the support. For this sample it is detected a higher particle size by XRD. On copper supported samples (CuZr), two reduction steps are detected that have been shifted to higher temperatures when copper is supported on zirconia stabilized with silica (CuZrSi). The lowest temperature peak is ascribed to highly dispersed copper oxide surface species, and the smaller the size of supported CuO particles, the easier they are reduced [16]. Rhodes and Bell [17] reported a greater interaction of copper oxide particles when are supported on tetragonal zirconia in comparison to monoclinic zirconia.

### 3.2. Activity testing

An important aspect to consider is not only the ethanol conversion but also the product distribution obtained for every catalyst studied. The increase in the number of carbon atoms in heavier alcohols introduces more complex pathways in reaction reforming mechanism and increases the number of by-products that it is possible to obtain. Fig. 5 compiles the product distribution obtained for Series 1. While NiZr and CoZr present high selectivity to hydrogen (>70%) (Fig. 5a), CuZr presents a selectivity to hydrogen lower than 40%. The presence of carbon monoxide (Fig. 5c) and methane (Fig. 5d) as reaction intermediates indicates the progress degree of the reforming process. From this standpoint carbon dioxide concentration close to 18% in the case of NiZr or CoZr indicates the progress of reforming and water gas shift reactions to obtain hydrogen and carbon dioxide as final products (Fig. 5b). The key to understand these results is obtained in Fig. 6 where the content of reaction by-products is represented. It is remarkable the presence of ethylene in product distribution for CuZr (Fig. 6a). In addition, the selectivity to acetaldehyde for CuZr achieves 30% (Fig. 6b) while the selectivity for NiZr and CoZr is negligible.

Fig. 7a represents the ethanol conversion versus time for nickel, cobalt and copper catalyst supported on zirconia at 700 °C, atmospheric pressure, and S/C ratio 4.8 during 15 h. It is noteworthy the total conversion obtained for nickel and cobalt catalysts, while for the copper ones, ethanol conversion starts to decrease when the catalyst sample is submitted to operation conditions.

Fig. 7b represents the ratio mol $H_2$/mol EtOH obtained versus time for the different catalysts supported on zirconia. NiZr

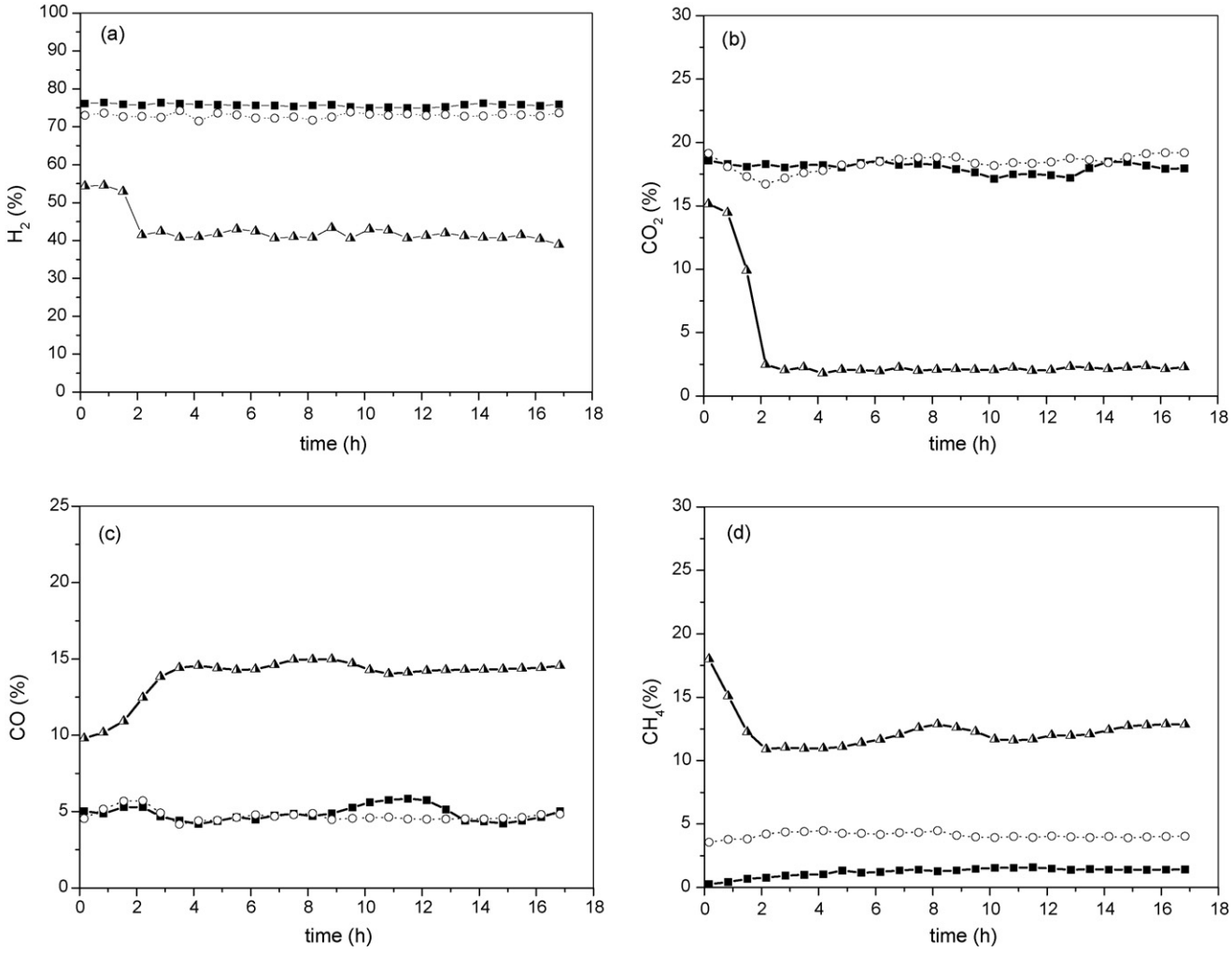


Fig. 5. Product distribution obtained for Series 1 catalysts: (a) hydrogen; (b) carbon dioxide; (c) carbon monoxide; (d) methane. (■) NiZr, (◯) CoZr, (◭) CuZr.

exhibits the highest efficiency. It is noteworthy that the value obtained by NiZr achieves 4.5 mol $H_2$/mol of ethanol fed to the reactor. This result represents an efficiency close to 81%, related to the equilibrium prediction for this reaction conditions, and it is in good agreement with the absence of by-product, opposite to CuZr catalyst which exhibits low hydrogen production efficiency. After 15 h in reaction mixture, nickel and cobalt catalysts exhibited a great stability.

For catalysts supported on zirconia stabilized with silica (Series 2), NiZrSi and CoZrSi catalysts achieve total ethanol conversion in the time range studied, while CuZrSi scarcely achieves 50% (Fig. 10a). This fact has a direct influence in product distribution (Figs. 8 and 9). For nickel and cobalt catalysts, hydrogen selectivity achieves values higher than 70% (Fig. 8a), that indicates the high progress degree of reforming process. This fact is demonstrable by analysing the selectivity to carbon dioxide and methane (Fig. 8b and d) that achieves values close to 20% and 4%, respectively. On the other hand, the selectivity to hydrogen for CuZrSi catalyst is really low and scarcely achieves 50%, value that was decreasing versus reaction time. This value is influenced by the presence of acetaldehyde in the by-product distribution (Fig. 9). It is a remarkable fact that the selectivity to ethylene achieves 8% (Fig. 9a).

The efficiency to hydrogen production is directly related to the product distribution. The use of zirconia stabilized with silica has diminished the hydrogen production from 4.5 mol $H_2$/mol EtOH for NiZr to 4 for NiZrSi. Similar result was obtained for CoZrSi, where hydrogen production was diminished from 4 mol $H_2$/mol EtOH for CoZr to 3.5 for CoZrSi (Fig. 10b).

## 4. Discussion

Ethanol steam reforming is a very complex reaction system where many reactions can take part in reaction mechanism [18]. At high temperature and water presence, ethanol can be dehydrogenated to produce acetaldehyde or dehydrated to produce ethylene as intermediate reaction products. It is observed that for copper supported catalysts, the main by-product obtained is acetaldehyde that comes from ethanol dehydrogenation (Figs. 6b and 9b). Goula et al. [19] demonstrated that ethanol dehydrogenation is feasible without catalyst by homogeneous reaction performed in a quartz tube reactor. Comás et al. [20] over Ni–Cu/$Al_2O_3$ catalyst demonstrated that ethanol reforming

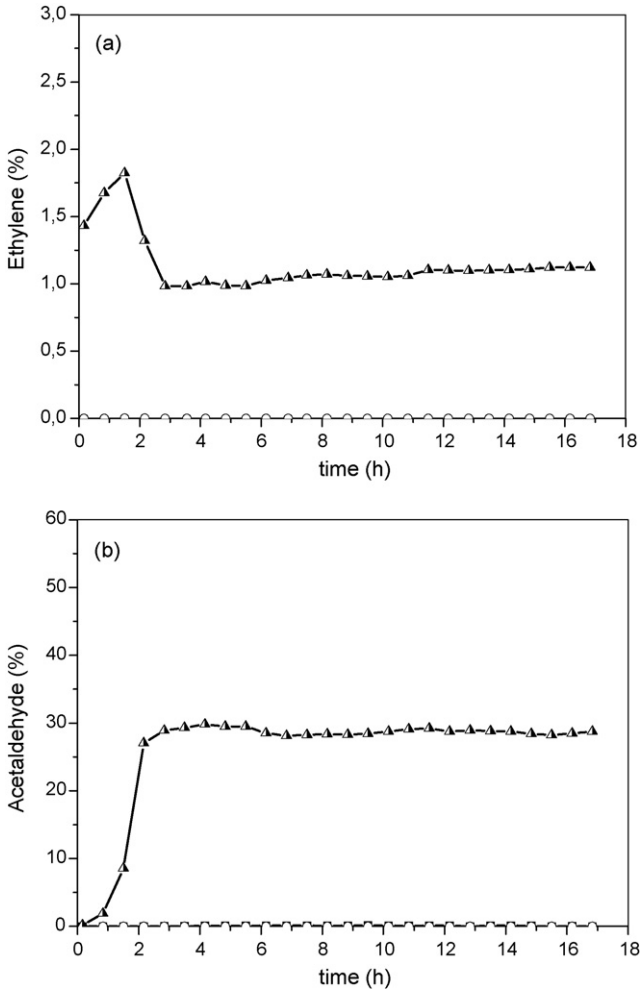


Fig. 6. By-product distribution obtained for Series 1 catalysts: (a) ethylene; (b) acetaldehyde. (■) NiZr; (◯) CoZr; (◭) CuZr.

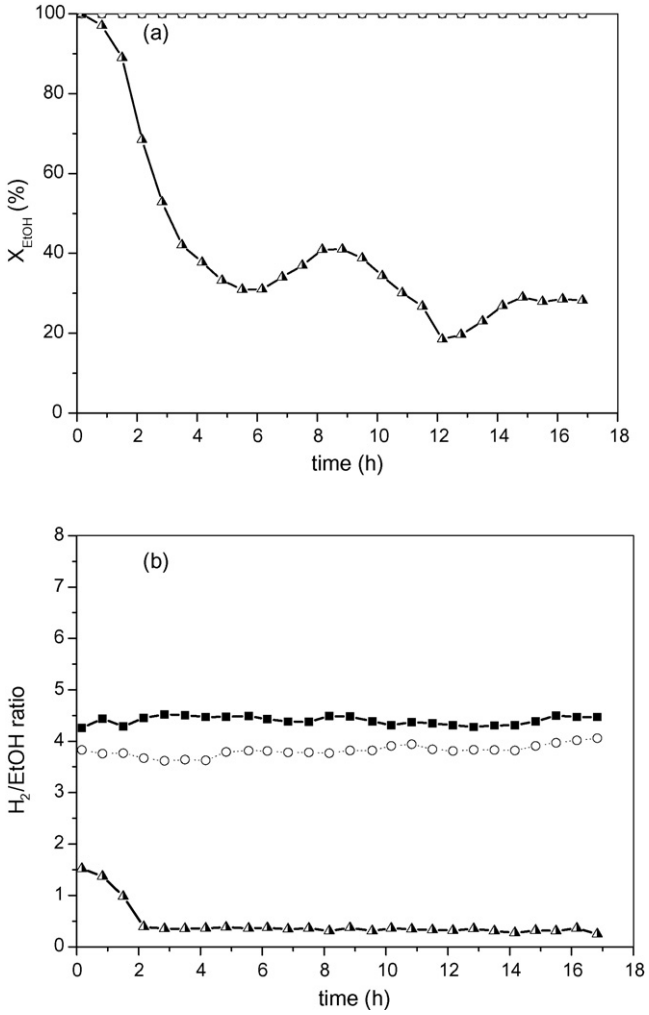


Fig. 7. Ethanol conversion (a) and $H_2$/EtOH ratio (b) for Series 1 catalysts: (■) NiZr; (◯) CoZr; (◭) CuZr.

proceeds via dehydrogenation reaction to obtain acetaldehyde. Acetaldehyde by decarbonylation reaction is transformed in methane, which is reformed to produce hydrogen and carbon monoxide. Mariño et al. [9] reported that the role of copper phase is to promote ethanol dehydrogenation and the nickel role is to activate acetaldehyde C–C bond to produce methane and carbon monoxide.

Results not presented showed that the increase of GHSV on nickel and cobalt catalysts improves the selectivity to acetaldehyde. This fact demonstrates that acetaldehyde is a reaction intermediate in nickel and cobalt zirconia supported catalysts.

In addition, copper based catalysts favour dehydration reaction to produce ethylene, fact detectable in Figs. 6a and 9a, where the evolution of ethylene content for the different catalysts studied is represented. Ethylene presence is associated to characteristic acid sites of alumina [21,23]. In this case, the increase of zirconia surface acidity by silica addition, improves ethylene production in copper supported catalysts (Fig. 9a). On the other hand, nickel and cobalt supported catalysts do not show ethylene in the product distribution, compound that could be reformed to produce methane, carbon dioxide and water [20].

Other important aspect is the support selection. Some authors have determined that the acidity of the support is a fundamental aspect to avoid dehydration reaction that can promote important deactivation processes by deposition of carbon on the active phase. Carbon is produced by ethylene decomposition or the Boudouard reaction [8]. Some authors have tried to modify the support surface acidity by introduction of alkaline modifiers such as potassium hydroxide deposited on alumina or MgO [6,9]. Other authors have prepared catalysts with basic support such as magnesium oxide [22,23] or zinc oxides [24], improving the catalyst behaviour to deactivation processes.

The addition of silica stabilizes the tetragonal phase that is observed in diffractograms obtained (Fig. 4) in comparison with non-stabilized zirconia which presents a monoclinic structure (Fig. 3). Nitrogen isotherm obtained at 77 K shows an increase of specific area for stabilized zirconia and diminishes the pore size obtained. The silica addition not only modifies the crystal structure and textural properties but also improves the surface acidity, remarkable aspect studied in bibliography. It is noteworthy that the catalysts supported on zirconia (Series 1) present

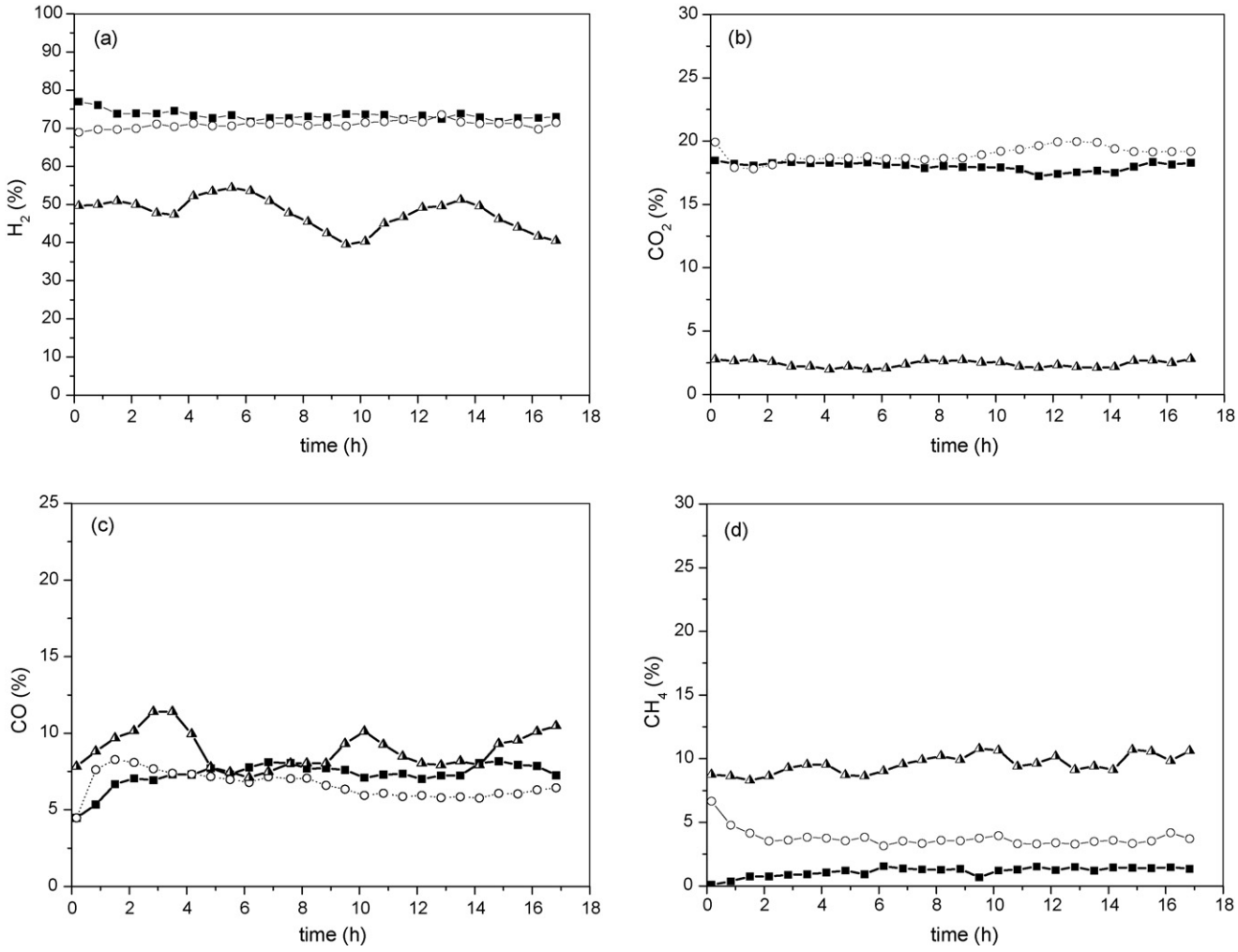


Fig. 8. Product distribution obtained for Series 2 catalysts: (a) hydrogen; (b) carbon dioxide; (c) carbon monoxide; (d) methane. (■) NiZrSi; (◯) CoZrSi; (◭) CuZrSi.

more efficiency to hydrogen production than zirconia stabilized with silica supported ones (Series 2).

It is observed that nickel supported catalysts exhibit more efficiency in hydrogen production (Fig. 7b) than cobalt supported ones. Several factors contribute to this fact: a low methane concentration in the products distribution, and higher contribution of water gas shift reaction, feasible in this type of catalysts. The presence of methane in the products distribution could have the origin in methanation reaction of carbon monoxide or carbon dioxide, that consumes 3–4 mol $H_2$/mol of carbon monoxide or carbon dioxide converted [8], or due to a lower shift of methane reforming reaction, reaction considered in the most of reaction mechanisms proposed for ethanol reforming [18,25]. Carbon monoxide hydrogenation is a reaction specially favoured at high temperature. This is a considerable reaction pathway when catalyst constitutes a high size catalytic bed, where thermal gradients presented are important due to the great ethanol reforming endothermicity. Nevertheless, this factor is negligible for the experimental conditions used in this study.

In this case, the water gas shift contribution is low, fact observed by comparison of carbon monoxide concentration for nickel and cobalt supported catalysts (Fig. 5c). Therefore, the methane is a reaction intermediate produced by acetaldehyde decarbonylation reaction. Methyl species adsorbed on the active phase can react to produce hydrogen and carbon monoxide. From this standpoint nickel supported catalysts are more active for methane reforming than cobalt ones (Figs. 5d and 8d). Nevertheless, Freni et al. [26] reported that Co/MgO was very active for methanation reaction in comparison to Ni/MgO. The cobalt properties are modified by support interaction [27]. From this standpoint, alumina suppresses methanation reaction and improves hydrogen production in comparison to cobalt supported on alumina.

### 4.1. Ageing experiments

An important experimental parameter to consider in bioethanol steam reforming is the influence of the ratio S/C in the steam reforming performance [28]. In this way, to vaporize water and increase the temperature to achieve the reforming temperature is a process that can limit energy efficiency of the ethanol reforming process. Ioanides [29] carried out a themodynamic study to evaluate the influence of S/C ratio in hydrogen production and reported that the limit S/C ratio to perform the

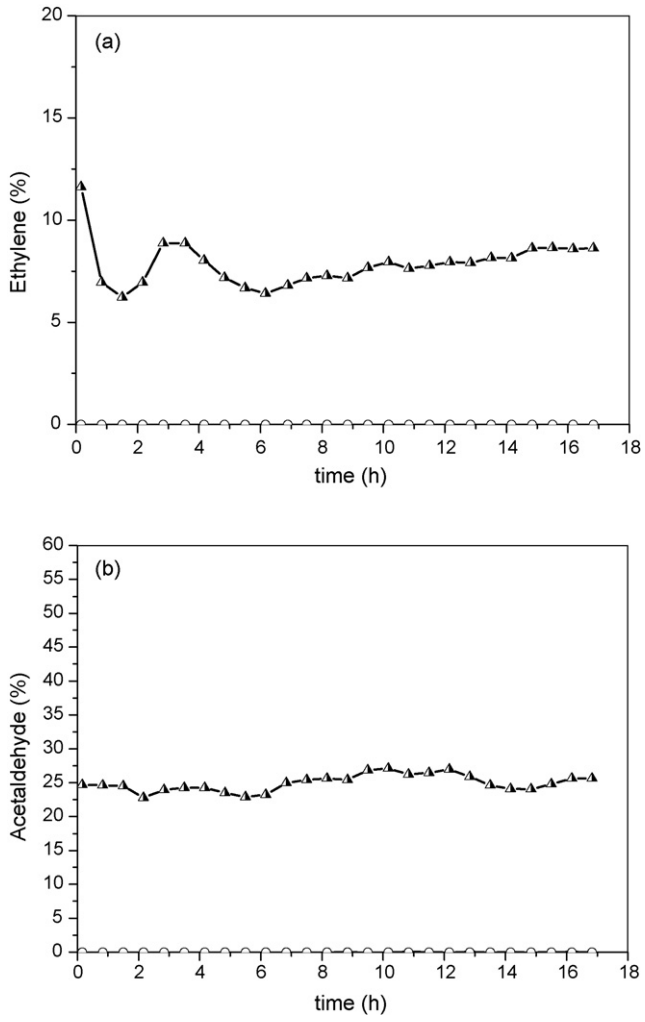


Fig. 9. By-product distribution obtained for Series 2 catalysts: (a) ethylene; (b) acetaldehyde. (■) NiZrSi; (◯) CoZrSi; (◭) CuZrSi.

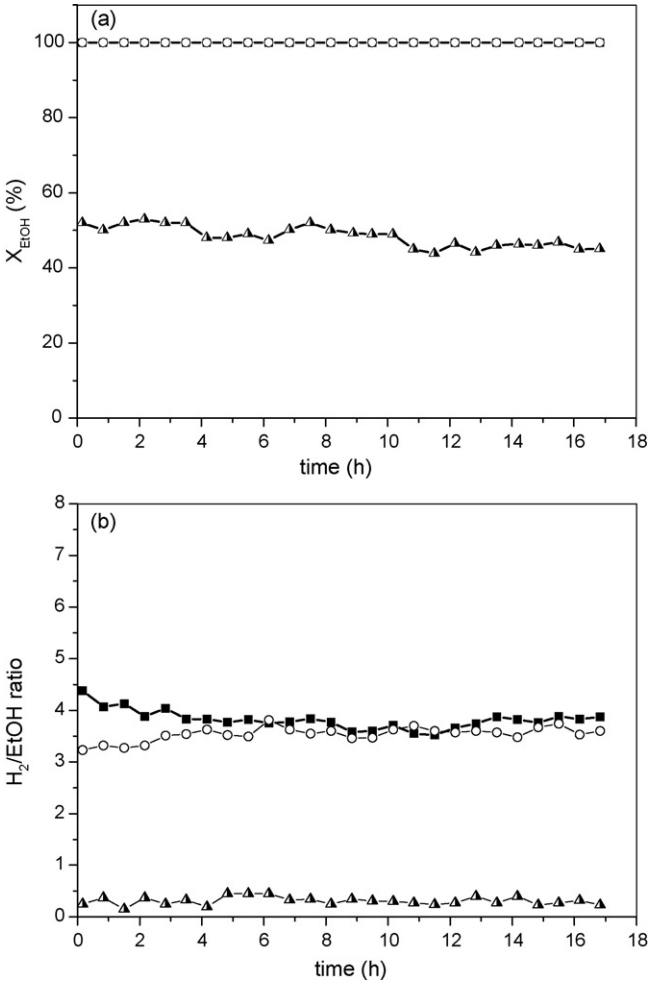


Fig. 10. Ethanol conversion (a) and $H_2$/EtOH ratio (b) for Series 2 catalysts: (■) NiZrSi; (◯) CoZrSi; (◭) CuZrSi.

ethanol steam reforming advantageously is 3. On the other hand, the decrease of the ratio S/C is limited by the carbon deposition phenomena on the active phase, responsible of deactivation processes in reforming catalysts. Fig. 11 shows the influence of the ratio S/C in NiZrSi catalytic performance. As thermodynamic equilibrium predicts a decrease in S/C ratio produces an increase in carbon monoxide concentration to achieve values close to 10% [30]. The increase of S/C ratio usually enhances methane reforming [29], nevertheless, the results obtained for NiZrSi, the influence of S/C ratio in methane product distribution is negligible. The main effect of S/C ratio diminish in NiZrSi is a lower participation of water gas shift reaction, that conduces to low carbon dioxide concentration and therefore the hydrogen concentration in the final product distribution is diminished.

The optimal S/C ratio to perform the ethanol reforming is conditioned to the final application where hydrogen needs to be supplied. For instance, for high, medium or low temperature fuel cell, the request for the final carbon monoxide concentration obtained in a fuel processor will be different. While high temperature fuel cells (SOFC, MCFC) are tolerant to high carbon monoxide concentration, low temperature fuel cell (PEMFC) must to operate with carbon monoxide concentration lower than 50 ppm. A high carbon monoxide concentration in the reformate stream must increase the dimension of water gas shift reactors to achieve an optimum carbon monoxide concentration (<1%) in order to perform the preferential oxidation stage.

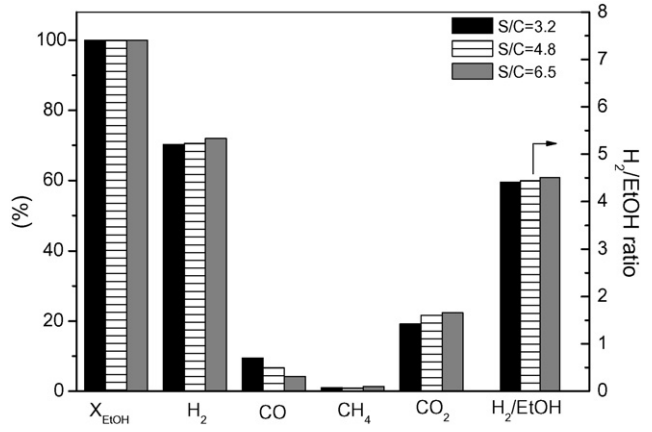


Fig. 11. Influence of S/C ratio on product distribution, ethanol conversion and hydrogen/ethanol ratio obtained on NiZrSi: (■) S/C = 3.2; (▤) S/C = 4.8; (▩) S/C = 6.5.

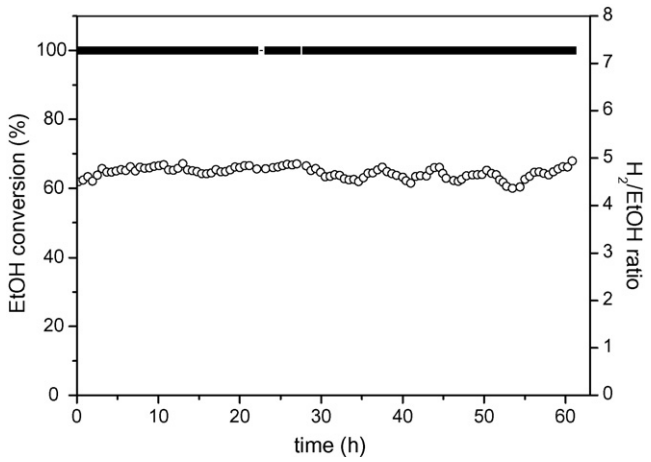


Fig. 12. Ethanol conversion and $H_2$/EtOH ratio obtained in long-term reaction experiments on NiZrSi. (■) ethanol conversion; (◯) hydrogen/ethanol ratio.

An important aspect to solve in heavier alcohol reforming is the resistance of the catalyst to deactivation processes. Low S/C in addition to high operation time produces catalyst deactivation. In literature there are few papers that present long-term catalytic tests to evaluate the resistance [19,30,31]. Fig. 12 shows the evolution of ethanol conversion and $H_2$/EtOH ratio obtained for NiZrSi catalyst operating at 973 K and S/C = 3.2. Catalyst presented 100% of ethanol conversion and very high hydrogen production, obtaining more than 4.5 mol $H_2$/mol of ethanol fed to the reactor. It is noteworthy the stability of NiZrSi catalyst after 60 h in reaction conditions with a really low S/C ratio, close to thermodynamic values where the carbon deposition is feasible. The product distribution obtained (Fig. 13) presents hydrogen concentrations higher than 70% in the time range studied. Two factors are responsible for this efficiency: low methane concentration presented in the product distribution due to the great progress of methane reforming and water gas shift reactions that enhance the final concentration of hydrogen and carbon dioxide.

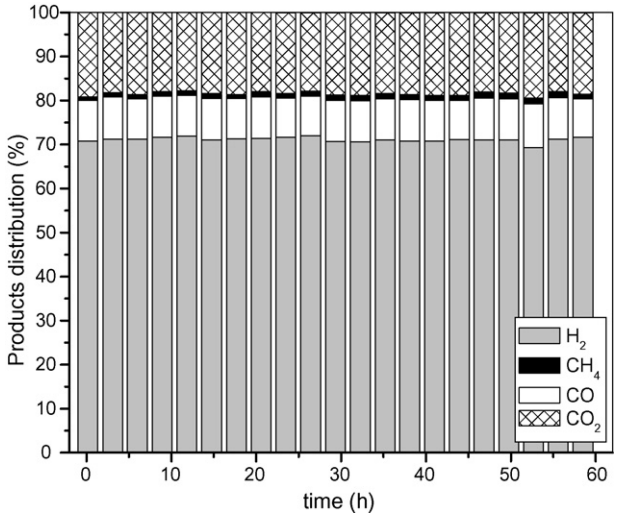


Fig. 13. Products distribution obtained in long-term reaction experiments on NiZrSi: (▩) hydrogen; (□) carbon monoxide; (■) methane; (▨) carbon dioxide.

## 5. Conclusions

The results obtained demonstrate that ethanol reforming presents a reaction mechanism where many by-products can be obtained. The election of the active phase determines the reaction pathway and therefore the products obtained in reforming process. Experimental results show that nickel and cobalt supported on zirconia exhibits high catalytic activity and stability for ethanol steam reaction without by-products. On the other hand, copper supported on zirconia exhibits high activity to ethanol dehydrogenation to yield acetaldehyde, being presented in products distribution ethylene that proceeds from ethanol dehydrogenation.

Opposite to acid supports such as alumina, the use of zirconia avoids ethylene production via ethanol dehydratation and its final decomposition to carbon on the active phase.

It is noteworthy the activity and stability of NiZrSi catalyst after 60 h in operation conditions at S/C ratio as low as 3.2, without deactivation signs and very high hydrogen production (4.5 mol $H_2$/mol EtOH). The results obtained in a long-term experiment, allows conclude the possibility of applying this catalyst in an ethanol processor to supply hydrogen to a fuel cell.

## References

[1] A.E. Lutz, R.S. Larson, J.O. Keller, Int. J. Hydrogen Energy 27 (10) (2002) 1103.
[2] W.H. Sholz, Gas Sep. Purif. 7 (1993) 131–139.
[3] J.T. Houghton, L.G. Meiro Filho, B.A. Callander, N.A. Harris Kattenberg, K. Maskell (Eds.), Climate Change 1995: The Science of Climate Change, Cambridge University Press, Cambridge, 1996, p. 572.
[4] T.A. Milne, C.C. Elamand, E.R. Evans. Hydrogen from biomass. State of the art and research challenges. Report IEA/H2/TR-02/001. International Energy Agency, 2001, pp. 1–78.
[5] Report US Department of Energy, DOE/GO-102000-0907, June 2000.
[6] F. Frusteri, S. Freni, V. Chiodo, L. Spadaro, O. Di Blasi, G. Bonura, S. Cavallaro, Appl. Catal. A: Gen. 270 (2004) 1–7.
[7] J.P. Breen, R. Burch, H.M. Coleman, Appl. Catal. B: Environ. 39 (2002) 65–74.
[8] A.N. Fatsikostas, X.E. Verykios, J. Catal. 225 (2004) 439–452.
[9] F. Mariño, G. Baronetti, M. Jobbagy, M. Laborde, Appl. Catal. A: Gen. 238 (2003) 41–54.
[10] J. Llorca, N. Homs, J. Sales, P.R. de la Piscina, J. Catal. 209 (2002) 306–317.
[11] A. Kaddouri, C. Mazzocchia, Catal. Commun. 5 (2004) 339–345.
[12] J. Rasko, A. Hancz, A. Erdohelyi, Appl. Catal. A: Gen. 269 (2004) 13–25.
[13] N. Iwasa, O. Yamamoto, R. Tamura, M. Nishikubo, N. Takezawa, Catal. Lett. 62 (1999) 179–184.
[14] H. Roh, K. Jun, W. Dong, J. Chang, S. Park, Y. Joe, J. Mol. Catal. A: Chem. 181 (2002) 137–142.
[15] L.F. Liotta, G. Di Carlo, G. Pantaleo, G. Deganello, Catal. Commun. 6 (2005) 329–336.
[16] G. Avgouropoulos, T. Ioannides, H. Matralis, Appl. Catal. B: Environ. 56 (2005) 87–93.
[17] M.D. Rhodes, A.T. Bell, J. Catal. 233 (2005) 198–209.
[18] M. Benito, J.L. Sanz, R. Isabel, R. Padilla, R. Arjona, L. Daza, J. Power Sources 151 (2005) 11–17.
[19] A.M. Goula, S.K. Kontou, P.E. Tsiakaras, Appl. Catal. B: Environ. 49 (2004) 135–144.
[20] J. Comás, F. Mariño, M. Laborde, N. Amadeo, Chem. Eng. J. 98 (2004) 61–68.
[21] J.R. Rostrup-Nielsen, N. Hojlund, in: J. Oudar, H. Wise (Eds.), Deactivation and Poisoning of Catalyst, Marcel Dekker, New York, Basel, 1985, p. 57.

[22] S. Freni, S. Cavallaro, N. Mondello, L. Spadaro, F. Frusteri, Catal. Commun. 4 (2003) 259–268.
[23] M.S. Batista, R.K.S. Santos, E.M. Assaf, J.M. Assaf, E.A. Ticianelli, J. Power Sources 124 (2003) 99–103.
[24] J. Llorca, P. Ramírez de la Piscina, J.A. Dalmon, J. Sales, N. Homs, Appl. Catal. B: Environ. 43 (2003) 355–369.
[25] I. Fishtik, A. Alexander, R. Datta, D. Geana, Int. J. Hydrogen Energy 25 (2000) 31–45.
[26] S. Freni, S. Cavallaro, N. Mondelo, L. Spadaro, F. Frusteri, J. Power Sources 4704 (2002) 1–5.
[27] F. Haga, T. Nakayima, H. Miya, S. Mishima, Catal. Lett. 48 (1997) 223–227.
[28] V. Klouz, V. Fierro, P. Denton, H. Katz, J.P. Lisse, S. Bouvot-Mauduit, C. Mirodatos, J. Power Sources 105 (2002) 26–34.
[29] T. Ioanides, J. Power Sources 92 (2001) 17–25.
[30] J. Sun, X. Qiu, F. Wu, W. Zhu, W. Wang, S. Hao, Int. J. Hydrogen Energy 29 (2004) 1075–1081.
[31] D.K. Liguras, D.I. Kondarides, X.E. Verykios, Appl. Catal. B: Environ. 43 (2003) 345–354.